

A generalized method for controlling end-tidal respiratory gases during nonsteady physiological conditions

Shawn M. O'Connor,^{1,2} Jeremy D. Wong,² and J. Maxwell Donelan²

¹School of Exercise and Nutritional Sciences, San Diego State University, San Diego, California; and ²Department of Biomedical Physiology and Kinesiology, Simon Fraser University, Burnaby, British Columbia, Canada

Submitted 28 March 2016; accepted in final form 13 September 2016

O'Connor SM, Wong JD, Donelan JM. A generalized method for controlling end-tidal respiratory gases during nonsteady physiological conditions. *J Appl Physiol* 121: 1247–1262, 2016. First published September 15, 2016; doi:10.1152/jappphysiol.00274.2016.—While forcing of end-tidal gases by regulating inspired gas concentrations is a common technique for studying cardiorespiratory physiology, independently controlling end-tidal gases is technically challenging. Feed-forward control methods are challenging because end-tidal values vary as a dynamic function of both inspired gases and other nonregulated physiological parameters. Conventional feedback control is limited by delays within the lungs and body tissues and within the end-tidal forcing system itself. Consequently, modern end-tidal forcing studies have generally restricted their analysis to simple time courses of end-tidal gases and to resting steady-state conditions. To overcome these limitations, we have designed and validated a more generalized end-tidal forcing system that removes the need for manual tuning and rule-of-thumb based control heuristics, while allowing for accurate control of gases along spontaneous and complicated time courses and under nonsteady physiological conditions. On average during resting, steady walking, and walking with time varying speed, our system achieved step changes in P_{ETCO_2} within 3.0 ± 0.9 (mean \pm SD) breaths and P_{ETO_2} within 4.4 ± 0.9 breaths, while also maintaining small steady-state errors of 0.1 ± 0.2 mmHg for P_{ETCO_2} and 0.3 ± 0.8 mmHg for P_{ETO_2} . The system also accurately tracked more complicated changes in end-tidal values through a bandwidth of 1/10 the respiratory (sampling) frequency, a practical limit of feedback control systems. The primary mechanism enabling this controller performance is a generic mathematical model of the cardiopulmonary system that captures the breath-by-breath relationship between inspired and end-tidal gas concentrations, with secondary contributions from reduced delays in controlled air delivery.

end-tidal forcing; cardiopulmonary model; hypoxia; hypercapnia

NEW & NOTEWORTHY

We have designed and validated an end-tidal forcing system that removes the need for manual tuning and control policies based on rules-of-thumb, while allowing for accurate control of gases along spontaneous and complicated time courses and under nonsteady physiological conditions. The principal new feature enabling this improved controller performance is its use of a generic mathematical model of the cardiopulmonary system to capture the relationship between inspired and end-tidal gas concentrations at each breath.

FORCING OF END-TIDAL GASES is a common experimental technique for studying cardiorespiratory physiology and function. The term end-tidal forcing (ETF) generally describes techniques that alter the composition of inspired gases for the

purposes of independently controlling the end-tidal partial pressures of oxygen (P_{ETO_2}) and carbon dioxide (P_{ETCO_2}), where the end-tidal partial pressures are those measured at the end of each breath. End-tidal partial pressures are a reliable proxy for the more difficult to measure arterial values (4)—end-tidal forcing thus provides indirect control of arterial blood gases. Perturbation of end-tidal gases has proven to be a useful paradigm for studying the role of arterial gases in the control of ventilation (24, 26), evaluation of cerebrovascular function (18), and simulating the detrimental effects of respiratory pathologies, such as sleep apnea (7).

Independently controlling end-tidal values with inspired gases is challenging for a number of technical and physiological reasons. First, during ETF, inspired gas concentrations are controlled by mixing and humidifying air from separate gas sources and end-tidal values are measured from sensors with relatively slow response times (>0.5 s). Delays in these processes prevent immediate alterations in inspired gases planned based on measured end-tidal values. Second, even rapid changes in inspired gases result in much slower end-tidal responses because the inspiratory gases are filtered by the much larger lung and body tissue volumes (12). Third, the relationship between inspired and end-tidal values depends on ventilation rate, cardiac output, and metabolic rate, which vary over time and between subjects (28). Finally, the autonomic control of ventilation, which is very sensitive to arterial blood gases, also works against external control of blood gases by adjusting ventilation in an attempt to return gas levels to baseline levels. Modern ETF systems, classified by use of either active or passive corrective feedback (see subsequent paragraphs for definitions of active and passive), address many of these challenges by restricting end-tidal control to step changes during steady-state and low-intensity (resting) conditions. This choice limits the complexity of the end-tidal response to inspired gases and allows heuristic planning of inspired concentrations to speed step transitions. Heuristic approaches compute inspired gases using rules of thumb gained through experience and may be sufficient under some circumstances such as step changes but are not necessarily generally appropriate for other controlled changes (e.g., ramps, sinewaves). We addressed these issues by modifying gas delivery hardware to reduce delays and modeling the cardiopulmonary system to allowing planning of inspired gas concentrations for a wide range of desired end-tidal time courses, including during nonsteady metabolic expenditure conditions.

Active feedback systems, otherwise known as dynamic end-tidal forcing systems, use computer control to assess the difference between desired, or reference, end-tidal values and measured end-tidal values on a breath-by-breath basis. These systems then automatically adjust inspired air concentrations to

Address for reprint requests and other correspondence: S. O'Connor, San Diego State Univ., School of Exercise and Nutritional Sciences, 5500 Campanile Dr., San Diego, CA 92182 (e-mail: soconnor@sdsu.edu).

compensate for this difference or error (13, 20). Computer-controlled feedback systems perform well in steady state because feedback excels at rejecting even small errors over time. However, feedback systems suffer from delays associated with measuring end-tidal values and delivering inspired air concentrations. These delays limit how effectively feedback control can reject end-tidal errors related to rapid changes in reference values or ventilation induced perturbations of measured values. Some active systems overcome the former limitation by incorporating a parallel feedforward controller that predicts necessary inspired gases to achieve reference end-tidal values either based on respiratory models (20) or predetermined heuristics (13). Active ETF systems have generally achieved step-like changes in end-tidal values in resting subjects within several breaths and maintained steady-state conditions with an absolute error of <1 mmHg and standard deviation of ~ 1 mmHg (13, 20).

An alternative to active ETF systems are passive systems, which avoid using computer-based feedback by designing the respiratory equipment to passively dampen perturbations in end-tidal values attributed to variations in ventilation rate (2, 10, 22). These passive systems, referred to as prospective end-tidal targeting systems, rely on sequential delivery of a preplanned control gas and previously exhaled gas within a single breath. Increased ventilation rates beyond baseline draw increasingly from the exhaled air reservoir, which contains gas roughly at the arterial blood gas levels. Therefore, only control gas participates in exchange within the lungs and end-tidal values are automatically stabilized against increases in ventilation rate (2, 22). This sequential delivery also reduces variations of respiratory gases within the lung and improves matching between end-tidal and arterial gas values. Passive ETF systems have achieved similar performance for step-like changes as active systems (22) in subjects at rest. However, passive systems have traditionally relied on preplanned estimations of required inspired gas and therefore cannot compensate for drifts in metabolic rate or rate of gas storage in body tissues (5), making them less accurate during nonsteady-state exercise conditions and over longer time scales.

While end-tidal step changes in at-rest subjects are suitable for a number of physiological investigations, current implementations of active and passive ETF systems are restricted to these experimental conditions. These implementations rely on control heuristics specific to step perturbations that would be unsuitable for other end-tidal time courses (e.g., ramp). These systems also assume that the parameters that affect the end-tidal response (e.g., ventilation rate, metabolic rate) are relatively constant, either by choices in feedback control parameters or by preplanned inspired gas concentrations. Ideal control parameters should vary as a function of the dynamic relationship between inspired and end-tidal values. Static controllers thus restrict end-tidal control to conditions of quasi-steady breathing and preclude testing under conditions of nonsteady exercise.

A more general approach would be useful for studies that require end-tidal control during nonsteady conditions and for which the reference time courses cannot be planned ahead of time. One of many potential applications is the control of end-tidal values during nonsteady exercise to estimate the role of blood gases in the hyperpnea response to exercise onset (6). A second application involves maintaining PET_{O_2} levels during

rapid changes in PET_{CO_2} induced by hyperventilation for the purposes of measuring cerebrovascular reactivity to hypocapnic CO_2 , a useful measure of cerebrovascular function (3, 5).

The purpose of this paper is to present the design and evaluation of a more generalized active end-tidal forcing system that improves upon limitations of existing systems. This generalized system removes the need for specific manual tunings and control heuristics, while allowing for accurate control of gases along spontaneous and complicated time courses, and under nonsteady metabolic expenditure conditions. The principal new feature enabling this improved controller performance is its use of a generic mathematical model of the cardiopulmonary system to capture the relationship between inspired and end-tidal gas concentrations. The parameters of this model are not static but are instead updated at each breath using measured respiratory parameters. The feedback component of our controller uses the updated model to retune its control parameters at each breath, improving control during nonsteady conditions. The feedforward component of our controller uses the updated model to design the appropriate inspired gas concentrations based on any reference end-tidal signal, improving tracking of spontaneous and complicated time courses. In addition to a new controller, we designed gas delivery hardware to reduce delays in controlled air delivery and to attain airflow rates suitable for testing during moderate exercise. To test the performance of our end-tidal forcing system, we used step changes in reference end-tidal gas values during both steady and nonsteady metabolic expenditure conditions and evaluated how quickly and accurately the actual end-tidal gases responded. We also evaluated controller performance using sine waves of increasing frequency, which are not typically achievable with manual tuning or heuristics-based control.

MATERIALS AND METHODS

In this section, we first describe our generalized ETF system design, beginning with the hardware and then followed by the software. We then describe the experimental conditions and analysis used to quantify system performance.

Hardware Design

We designed the gas delivery hardware to provide controlled concentrations of inspired air with high accuracy and low delay. We based the initial design on a compact end-tidal forcing system from Koehle et al. (13), which consists of medical grade compressed gas tanks (air, nitrogen, oxygen, and carbon dioxide) regulated to supply gas via solenoid valves to a mixing and humidification chamber and then to a reservoir bag from which the subjects drew inspired air (Fig. 1A). The volume of air delivered at each breath matched the previous breath's tidal volume to maintain sufficient reserve volume (~ 1.5 liters) in the reservoir bag. This design requires comparatively low inspiratory flow rates because subjects inhale from a closed intake system, leaving no unused gas mixture. We additionally modified the design to increase and stabilize flow rates of air delivery and reduce delays in delivering controlled air to the subject, as described below.

Pneumatic hardware provided maximum flow rates of mixed air of 110 l/min, which we estimated to exceed the maximum subject ventilation rate when exposed to hypercapnic and hypoxic conditions during moderate exercise (14). Pressure regulators (Blueshield 60 Series; Air Liquide) connect to the gas tanks and provide a 60 psi source for the solenoid valves. Solenoid valves (model 8262G202; ASCO) regulate flow for each of four air channels in an on/off manner

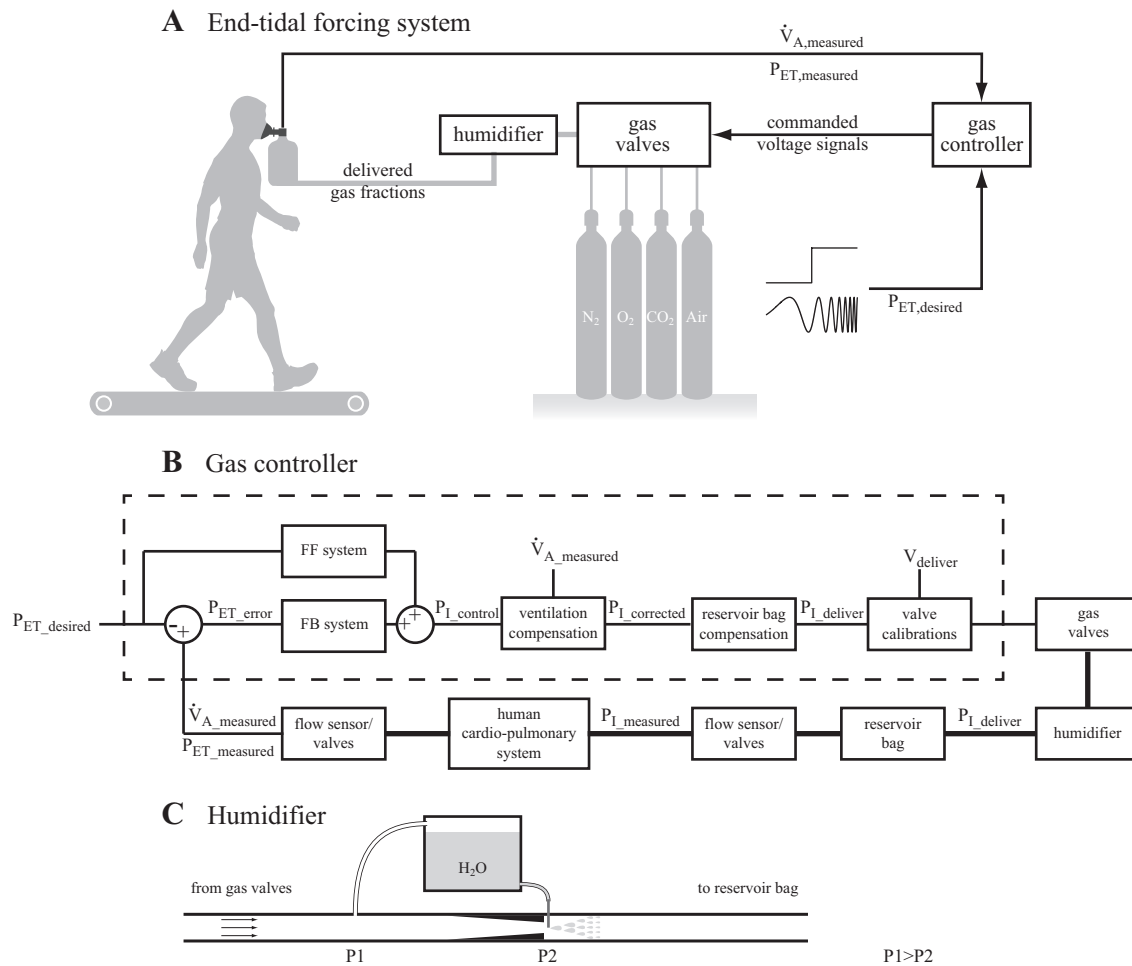


Fig. 1. End-tidal forcing system design and controller diagram. *A*: we have built a custom end-tidal forcing system that controls the end-tidal partial pressures of oxygen (P_{ET,O_2}) and carbon dioxide (P_{ET,CO_2}) by varying the gas composition of inspired air. The system consists of compressed gas sources (air, oxygen, nitrogen, and carbon dioxide) connected via four electronically controlled valves to humidifier and then an inspiratory reservoir bag from which the participant breathes. Subjects were outfitted with a respiratory mask that connects to the reservoir bag and captures inspired and expired air for measurement. *B*: diagram of gas controller implemented within end-tidal control loop. A real-time control system compares measured end-tidal gas partial pressures with reference pressures, chooses inspired air proportions to minimize the differences based on feedforward and feedback control laws, compensates for ventilation adaptations and reservoir bag contents, and computes the timing of valve opening to provide the appropriate gas mixture to the subject. *C*: diagram of humidifier.

and were sized to achieve a small pressure drop across the valve (<1 psi) at 60 psi and for peak flow conditions. The oxygen line solenoid valve was cleaned and guaranteed for oxygen service. We also installed brass orifices (E-63-BR air and nitrogen lines; EIJLC-40-2-BR oxygen line; O’Keefe Controls) downstream of the solenoid valves to regulate and stabilize the airflow against changes in pressure downstream of the orifices, which varies with humidification level, volume of the reservoir bag, and inhalation rate. The four air channels were then merged into a single tube before entering the humidification unit. The solenoid valves were opened and then closed once per breath cycle to deliver a burst of air into the respiratory bag. We calibrated each channel by varying the length of time the corresponding solenoid valve was open and measuring the volume of air delivered. The relationship between valve open duration and delivered air volume served as the calibration function which the real-time controller used to select the valve open durations at each breath based on the desired delivery volume of each gas.

End-tidal feedback control performance suffers from delays in both measuring end-tidal values and altering them through the delivery of inspired air concentrations. We designed system components to minimize these delays. Measures of end-tidal values are delayed because the respiratory gas analyzer (\dot{V}_{max} ; SensorMedics, Yorba Linda, CA)

must transport gas from the mouth to the oxygen and carbon dioxide sensors and because these sensors have finite response times. The total sensing delay of ~ 0.65 s for our oxygen sensor occupies a significant fraction of a typical inhalation period and therefore is a significant factor when designing the software controller. We therefore focused on two other modifiable delays associated with controlled air delivery. Filtering delay is the delay associated with changing the contents of the reservoir bag and occurs because new air entering the reservoir bag mixes with ~ 1.5 liters of residual air maintained in the reservoir bag. We reduced filtering effects by maintaining a minimal volume of air in the bag and by modeling and compensating for this gas composition when regulating incoming air (see *Software Control Design*). Transit delay defines the time from when air exits an open solenoid valve to when it enters the reservoir bag. Our design minimized the two largest sources of transit delay: humidification and air tubing volume. Transit delay was minimized during the humidification process by injecting water vapor directly into the compressed air stream, analogous to the carburetor fuel injection of older automobile engines (Fig. 1C). Briefly, a water bottle was connected to and pressurized by the merged air stream. The bottom of the water bottle drained into intravenous tubing with a 25 g hypodermic needle, which was inserted into the merged airline downstream of the water bottle.

The tubing was narrowed at this location to create a pressure differential between the water bottle and needle tip with air flow, injecting water directly into the compressed air stream and humidifying the air to ~50% relative humidity. This design differs significantly from previous humidification systems, which bubble air through a water container (13) or medical humidifier (22), both at the cost of significant dead space and thus transit delay. We also minimized transit delay by limiting the length of all tubing and selecting the inner diameter to be as small as possible without restricting air flow. Polyethylene tubing [1/4-in. inner diameter (ID), 3/8-in. outer diameter (OD)] connected flow equipment upstream of the humidifier. Nalgene tubing (1/4-in. ID) was used to connect the humidifier to the reservoir bag.

The system delivered gas to subjects through a facemask (V2 Mask; Hans Rudolph, Shawnee, KS) connected to a two-way flow sensor and gas analyzer (Vmax; SensorMedics). We chose facemasks over mouthpieces to allow more natural breathing from both nose and mouth and to allow subjects to verbally communicate with the experimenter. The end of the flow sensor connected to a two-way nonbreathing valve (NRB 2700; Hans Rudolph), with the expiratory port open to the atmosphere and the inspiratory port connected to the reservoir bag.

An Analog Interface Pod of the Vmax metabolic system provided analog output signals representing the instantaneous partial pressures of oxygen (PO₂) and carbon dioxide (PCO₂), as well as instantaneous inspiratory and expiratory flow rates. A finger pulse oximeter (Nonin 7500; Nonin Medical, Plymouth, MN) provided arterial oxygen saturation (SaO₂) and heart rate. A real-time control system (Simulink Real-Time Workshop; The Mathworks, Natick, MA) acquired all variables at 240 Hz using an analog-to-digital converter (National Instruments). Measured respiratory signals determined inspiration and expiration timing events and minute expired ventilation (\dot{V}_E), tidal volume (VT), and respiratory frequency (f_R). We defined the end-tidal partial pressures of oxygen (PET_{O₂}) and carbon dioxide (PET_{CO₂}) as the local minimum and maximum values of PO₂ and PCO₂, respectively, at the expiration phase of each breath.

Software Control Design

The conceptual goal of the computer control system is to achieve reference end-tidal time courses by designing a breath-by-breath time course of inspired gases. Changes in ventilation rate and metabolic rate are treated as unknown disturbances that perturb the end-tidal values. Feedback control is a superior strategy for such disturbances (17). However, feedback systems are sensitive to noisy or delayed sensed signals (i.e., end-tidal values) and to delays in delivering the input to the system (inspired gas levels). End-tidal values are generally noisy because of breath-by-breath ventilation variations. As discussed in the previous section, the control system computes a designed inspired concentration for the subsequent inhalation after measured end-tidal values at exhalation but delivery of this inspired air is delayed by a significant breath fraction. Although sensitive to unknown disturbances, feedforward systems are generally robust in the presence of such time delays (17). Therefore, a feedforward control component was added in parallel with the feedback pathway. This feedforward controller adjusted the inspired gas concentrations based on predicted requirements for achieving the time course of the reference values (20). Here, we describe model development and controller design for PET_{CO₂} control (see APPENDIX). A similar process informed PET_{O₂} controller design but is not presented in detail here.

We employed several unique software control improvements over existing ETF systems. We used a mathematical model of the cardiopulmonary system, updated at each breath using measured respiratory parameters, to plan feedforward and feedback control parameters that also varied from breath to breath. Assuming equivalence of end-tidal and arterial values, the controller takes the form,

$$PI_{CO_2\text{-control}} = f_{FF}(Pa_{CO_2,\text{desired}}) + f_{FB}(Pa_{CO_2,\text{error}}) \quad (1)$$

where $PI_{CO_2\text{-control}}$ is the inspiratory partial pressure of CO₂ planned by the controller, f_{FB} is the feedback component of the controller that varies as a function of the arterial error, and f_{FF} is the feedforward component that varies as a function of reference values. In the Laplace domain, the controller takes the form,

$$PI_{CO_2\text{-control}}(s) = C_{FF}(s)Pa_{CO_2,\text{desired}}(s) + C_{FB}(s)Pa_{CO_2,\text{error}}(s) \quad (2)$$

where s is a complex frequency variable called the Laplace variable. An additional control component adjusted inspired concentrations to further improve compensation for end-tidal perturbations due to changes in measured minute alveolar ventilation \dot{V}_A (see *Measurement of Model Parameters* in APPENDIX). This ventilation compensation function, f_{VC} , produced a corrected inspiratory partial pressure, $PI_{CO_2\text{-corrected}}$.

$$PI_{CO_2\text{-corrected}} = f_{VC}(PI_{CO_2\text{-control}}, \dot{V}_A) \quad (3)$$

The cardiopulmonary model describes the arterial blood gas response to changes in inspired gas. As a transfer function, the model for CO₂ takes the form,

$$P(s) = \frac{Pa_{CO_2}(s)}{PI_{CO_2}(s)} = \frac{T_1(T_3s + 1)}{T_1T_2T_3s^2 + (T_1T_2 + T_1T_3 + T_2T_3)s + T_1} \quad (4)$$

where the function is parameterized by physiologically relevant timing parameters,

$$T_1 = \frac{V_{ACO_2}}{863\dot{Q}K_{CO_2}}, T_2 = \frac{V_{ACO_2}}{\dot{V}_A}, T_3 = \frac{V_{TCO_2}}{\dot{Q}} \quad (5)$$

and where T_1 , T_2 , and T_3 represent mean residence times associated with blood perfusion of the lung, air perfusion of the lung, and blood perfusion of the body tissue, respectively. V_{ACO_2} and V_{TCO_2} are the effective storage volume of the lung and body tissues with respect to CO₂, \dot{Q} is the cardiac output, \dot{V}_A is the minute alveolar ventilation, and K_{CO_2} is the slope of the CO₂ dissociation curve. Volume parameters are estimated based on subject age, height, and resting tidal volume, while the timing parameters are dynamically updated at each breath based on a five breath running median filter for \dot{V}_A and estimation of \dot{Q} (see APPENDIX). While the model assumptions and simplifications do reduce the accuracy of arterial gas predictions, a perfect model is not necessary to achieve successful control as feedback control is particularly suited to compensate for control errors induced by model inaccuracies.

The feedforward controller plans inspired gas values based only on reference arterial time courses and is equivalent to using an inverse of the cardiopulmonary transfer function. However, since $P(s)$ is a proper transfer function (the degree of the denominator is greater than the degree of the numerator), inversion results in a function that grows unbounded for high frequencies inputs (e.g., step changes). We therefore multiplied the inverted system by a low pass filter with filter time constant τ chosen to equal the smallest timing parameter (T_1) to reduce high frequency sensitivity while minimizing distortion of the plant dynamics. For implementation in the end-tidal controller, this continuous feedforward controller was converted to a discrete model with a one breath sampling period.

$$C_{FF}(s) = \frac{1}{P(s)} \frac{1}{\tau s + 1} = \frac{T_1T_2T_3s^2 + (T_1T_2 + T_1T_3 + T_2T_3)s + T_1}{T_1(T_3s + 1)(T_1s + 1)} \quad (6)$$

The feedback controller plans inspired gas values based on the error between reference and measured arterial values using a standard proportional-integral (PI) controller,

$$C_{FB}(s) = K_P + K_I/s \quad (7)$$

where K_P and K_I are the proportional and integral gains, respectively. We chose these gains based on plant model dynamics using standard design rules that seek a balance between fast rejection of errors and closed-loop stability. We further simplified the plant model (Eq. 4) so as to use standard first order tuning rules to parameterize the feedback gains (see APPENDIX). With the use of the second method of Zeigler-Nichol's PI tuning (30), the proportional and integral gains are a direct function of the model parameters,

$$K_P = \frac{0.9T_2}{T_B} \quad K_I = \frac{0.9T_2}{3.3T_B^2} \quad (8)$$

and where T_B is one respiratory period. The feedback parameters were then tested and varied in simulation to determine whether parameters based on the Ziegler-Nichols criteria were suitable when combining feedback and feedforward control. Based on simulations of step changes in reference arterial values, we found that both feedback parameters should be divided approximately by 2 to limit overshoots to <5%. For implementation in the end-tidal controller, this continuous feedback controller was converted to a discrete model with a one breath sampling period.

Active ventilation compensation accounts for how changes in \dot{V}_A perturb end-tidal values, whether due to chemoreceptor responses or changes in metabolic rate, and adjusts the inspired air concentrations to compensate. While the feedback controllers can correct for these perturbations, its control parameters are not specifically tuned based on a cardiopulmonary system with \dot{V}_A as the input. Therefore, we adopted a ventilation compensation function to separately account for changes in measured \dot{V}_A ,

$$P_{\text{ICO}_2\text{-corrected}} = \left(P_{\text{ICO}_2\text{-control}} \cdot \dot{V}_A^* + P_{\text{aCO}_2\text{-measured}} \cdot (\dot{V}_A^* - \dot{V}_A) \right) / \dot{V}_A \quad (9)$$

where \dot{V}_A^* is the baseline minute alveolar ventilation. Since \dot{V}_A above baseline increases the inspiratory gas available for exchange in the lungs, the ventilation compensation function correspondingly increases the proportion of the inspired gas at the measured arterial value, gas that theoretically does not contribute to gas exchange in the lung. For example, \dot{V}_A increases that follow controlled increases in P_{ETCO_2} would temporarily lower P_{ETCO_2} until the feedback controller can compensate by increasing the inspired CO_2 concentration. The ventilation compensation function automatically increases inspired CO_2 concentration (increases inspired proportion at arterial value) based on measured \dot{V}_A . To reduce the effects of breath-by-breath variations in \dot{V}_A , the ventilation compensation uses a five-breath median average of \dot{V}_A .

Finally, the air delivered by the solenoid valves, $P_{\text{ICO}_2\text{-deliver}}$, is then adjusted to take into account the air concentration remaining in the reservoir bag, $P_{\text{ICO}_2\text{-reservoir}}$, so that the mixed concentration equals $P_{\text{ICO}_2\text{-corrected}}$ (Eq. 9).

$$P_{\text{ICO}_2\text{-deliver}} = \left(P_{\text{ICO}_2\text{-corrected}} \cdot (V_{\text{deliver}} + 1.5) - 1.5 \cdot P_{\text{ICO}_2\text{-reservoir}} \right) / V_{\text{deliver}} \quad (10)$$

The volume of air delivered, V_{deliver} , at each breath was matched to the measured tidal volume of the previous breath to maintain a sufficient reserve volume (~1.5 liters) in the reservoir bag after each inhalation.

Study Design

Six volunteers participated in this study (3 male, 3 female, aged 27.7 ± 3.0 yr; body mass 65.7 ± 7.9 kg; mean \pm SD). All were healthy adults with no known history of cardiovascular, neurological, or respiratory disease or impairments affecting daily walking function. Simon Fraser University's Office of Research Ethics approved the protocol and all subjects gave written informed consent before participation.

Sitting baseline data were first recorded for 7 min as subjects sat upright, wore the facemask, and breathed a normal air mixture provided by the ETF system. This period allowed the subject to acclimate to the experimental setup and any increase in inspiratory resistance associated with the use of the facemask and nonbreathing valve. We took as baseline measures the steady-state values during the last 3 min of this phase. Subjects then walked on a treadmill at 1.25 m/s while again breathing a normal air mixture to allow acclimation to walking while wearing the respiratory and end-tidal forcing equipment. This walking baseline trial lasted 7 min or until the subjects had achieved steady-state ventilation for at least 3 min, with the last 3 min used to determine baseline walking parameters. For both the sitting and walking baseline conditions, we quantified mean P_{ETO_2} , P_{ETCO_2} , \dot{V}_E , and \dot{V}_T . We then updated the cardiopulmonary model parameters based on these measured parameters and updated corresponding feedforward and feedback control parameters (see APPENDIX).

To gauge system performance, we then had subjects complete four experimental trials, covering three metabolic expenditure conditions and two types of end-tidal time courses. Metabolic expenditure conditions involved sitting at rest, walking at 1.25 m/s, and walking at a sinusoidally varying speed over a range of 1.1 to 1.4 m/s and with a period of 120 s. In the latter condition metabolic cost varied by approximately $\pm 11\%$ relative to the cost at 1.25 m/s (29). The first end-tidal scheme used an abbreviated protocol from Koehle et al. (13) and applied a sequence of independent step changes in P_{ETO_2} and P_{ETCO_2} (Table 1). The second scheme applied independent changes in P_{ETO_2} and P_{ETCO_2} in the form of sine waves of increasing frequency, referred to as a chirp signal. The chirp signals had mean values of +0 mmHg and +4 mmHg relative to baseline levels and amplitudes of 40 mmHg and 4 mmHg for P_{ETO_2} and P_{ETCO_2} , respectively. The end-tidal signal began 240 s into the trial at a frequency of 1/900 Hz and ended at time 900 s with a frequency of 1/10 Hz, or roughly 1/5 of the maximum expected respiratory frequency of 0.5 Hz.

Each trial served as a unique validation of the end-tidal system. An important consideration when studying physiological responses to changing blood gases is the ability to control confounding gas levels independently (e.g., O_2 levels are a confound when studying reactivity of ventilation to CO_2). *Trial 1* (Sitting, Step signals) tested precise and independent control of P_{ETO_2} and P_{ETCO_2} despite large changes in \dot{V}_E during steady, resting conditions. *Trial 2* (Steady walking, Step signals) verified control of independent step changes during conditions with higher metabolic rate and higher variability in \dot{V}_E . *Trial 3* (Nonsteady waking, step signals) tested the generality of the system and its ability to control during nonsteady exercise. Finally, *trial 4* (Nonsteady walking, chirp signals) validated control of end-tidal time courses that are more complicated than step changes and that mimic spontaneous profiles that limit the success of heuristic-based control approaches. The high-frequency portions of the chirp signal also tested the limits of the end-tidal control performance and provided a redundant confirmation of the step change performance. While the *trial 1* conditions are routine in end-tidal control experiments, the conditions of *trials 2-4* have not yet been tested in previous studies.

In all trials, we constrained blood gas levels within an established safe range ($P_{\text{ETCO}_2} < +8$ mmHg, $P_{\text{ETO}_2} > 55$ mmHg) (13). Both the subject and the experimenter had immediate access to an emergency stop button to cut off the controlled gas to the subject and deliver oxygen rich air. Monitored arterial oxygen saturation also automatically triggered the emergency stop ($\text{SaO}_2 < 75\%$).

Table 1. Protocol for independent step changes in P_{ETO_2} and P_{ETCO_2}

	240 s	120 s				
P_{ETO_2} , mmHg	–	–	–40	–40	–40	–
P_{ETCO_2} , mmHg	–	+7	+7	+4	–	–

Analysis

We used standard techniques from system identification to quantify system performance. We used the step perturbation trials to identify timing and accuracy parameters of the controlled end-tidal response for the given gas undergoing the step change. Timing parameters quantified how quickly the system responded to changes in reference values and accuracy parameters quantified how well the system reduced error between reference and measured end-tidal values. Performance was quantified for both steady sitting and walking and nonsteady walking. We identified these parameters using reference end-tidal time courses as the input and the measured end-tidal responses as the output of a second-order system with time delay (23). Fitting the data to such a model allowed precise extraction of time domain performance parameters from relatively noisy end-tidal data. A second order system was the simplest model that described the average response to a step input (i.e., the tendency of the end-tidal values to overshoot the reference value before reaching the reference value in steady state). The initial rapid behavior was quantified by time delay and rise time. Time delay was defined as the time required for the measured end-tidal values to cross 10% of the change in reference end-tidal value after the step change. Rise time was defined as the time required for the measured end-tidal values to cross 90% of the change in reference end-tidal value after the time delay. Settling time quantifies the slower settling behavior and is defined as the time required to reach and stay within 10% of the final value after the time delay. Maximum overshoot defines the maximum peak value of the end-tidal response measured relative to the reference end-tidal value (17). Steady-state error is defined as the difference between reference and measured end-tidal values after the rise time. Steady-state variability is defined as the standard deviation of the end-tidal values after the rise time. The identified parameters minimized the sum of the squared error between the model predictions, based on the step and chirp inputs, and the measured end-tidal outputs. To implement this system identification, and generate estimates and confidence bounds on the parameter values over all subjects, we used MATLAB's `idgrey.m` and `pem.m` functions.

For the chirp perturbations we used frequency response analysis to measure the controller gain and phase lag performance criterion as a function of reference signal frequency. This was accomplished by using MATLAB's `tffestimate.m` function with the reference end-tidal time courses as the input and the measured end-tidal responses as the output. Signals were first interpolated at 1/2 Hz, the approximate maximum respiratory frequency measured, to provide regularly sampled signals to the algorithm. From the gain-frequency relationship, we identified the system bandwidth, or frequency at which the measured end-tidal values are attenuated by 3 dB (gain = 0.707). We also identified a more conservative measure of bandwidth, where the gain falls below -0.92 dB (gain = 0.9), and the system achieves 10% error. We also identified the frequency at which the phase lag exceeded 45°, the theoretical frequency at which the coefficient of determination (r^2) between the reference and measured end-tidal values falls below 50%. While the system performance parameters may be identified from step responses alone, chirp perturbations served to validate those findings while demonstrating tracking of an end-tidal time course not possible for most ETF systems.

Paired *t*-tests determined significance between parameters measured during baseline sitting and steady state walking. One-way repeated-measures ANOVA determined whether ventilation parameters and step performance parameters differed significantly between the step trials (*trials 1–3*). Post hoc comparisons were performed as paired *t*-tests with Bonferroni correction. All analysis and statistical computations were performed in Matlab with a maximum Type I error rate (α) of 0.05. Values are presented as mean \pm SD unless otherwise stated.

RESULTS

Summary

Our generalized ETF system successfully controlled end-tidal values along independent time courses during varying metabolic expenditure conditions. On average, the system achieved step changes in P_{ETCO_2} within 3.0 ± 0.9 breaths and P_{ETO_2} within 4.4 ± 0.9 breaths (Figs. 2 and 3; Tables 2 and 3). The system also limited steady-state errors to 0.1 ± 0.2 and 0.3 ± 0.8 mmHg for P_{ETCO_2} and P_{ETO_2} , respectively, despite two- to threefold increases in \dot{V}_E over the course of the step trials and despite variations in walking speed during *trial 3*. Furthermore, the system achieved chirp signal time courses with minimal gain variation over the tested bandwidth.

Baseline Conditions

We used ventilation parameters established during the baseline trials to construct standing and walking specific models of respiration for planning feedforward and feedback control parameters. Average P_{ETCO_2} significantly increased from 35.0 ± 4.6 to 37.8 ± 4.6 mmHg (mean \pm SD, $P = 0.04$) during the sitting and walking baseline trials, respectively, whereas P_{ETO_2} significantly decreased from 104.0 ± 4.7 to 100.4 ± 4.5 mmHg ($P = 0.04$). Average \dot{V}_E significantly increased from 10.1 ± 1.2 to 25.6 ± 2.3 l/min ($P = 3e-5$) between sitting and walking. Since the feedback gains are approximately inversely proportional to \dot{V}_E , this 2.5-fold increase between these metabolic expenditure conditions indicates that the appropriate feedback gains also decrease by this same factor.

Minute Ventilation During Control (Trials 1–3)

Average \dot{V}_E over the period of end-tidal control increased by a factor of 2.2 ± 0.5 , 1.7 ± 0.2 , and 1.7 ± 0.2 over the corresponding baseline conditions for *trials 1–3*, respectively. The average \dot{V}_E during the most hypercapnic (+7 mmHg P_{ETCO_2}) and hypoxic (-40 mmHg P_{ETO_2}) portion of the trials increased by respective factors of 2.7 ± 0.7 , 2.0 ± 0.3 , and 2.0 ± 0.3 . The appropriate feedback gains then approximately decrease by these same factors within single trials. These large changes in \dot{V}_E also require significant controller effort to maintain end-tidal values against these perturbations. Trial number significantly influenced variability in \dot{V}_E (as measured by standard deviation, $P = 0.027$), with respective values of 5.2 ± 0.9 , 7.6 ± 1.6 , and 8.1 ± 1.9 l/min, and which tends to increase end-tidal variability and thus error.

Step P_{ETCO_2} Performance (Trials 1–3)

For all trials where step changes in P_{ETCO_2} were controlled, measured end-tidal values responded with an average time delay of 0.5 ± 0.5 breaths and an average rise time of 2.5 ± 0.7 breaths (Table 2). P_{ETCO_2} tended to overshoot reference values by 1.0 ± 0.8 mmHg (13.5% overshoot) before settling within 8.2 ± 6.0 breaths. The average standard deviation for P_{ETCO_2} after the rise period was 0.8 ± 0.2 mmHg, corresponding to a $1.7 \pm 0.4\%$ coefficient of variation. The mean value after the rise period was 0.1 ± 0.2 mmHg above the reference values and this error was not significantly different from zero ($P = 0.17$). These metrics include the time period where P_{ETO_2}

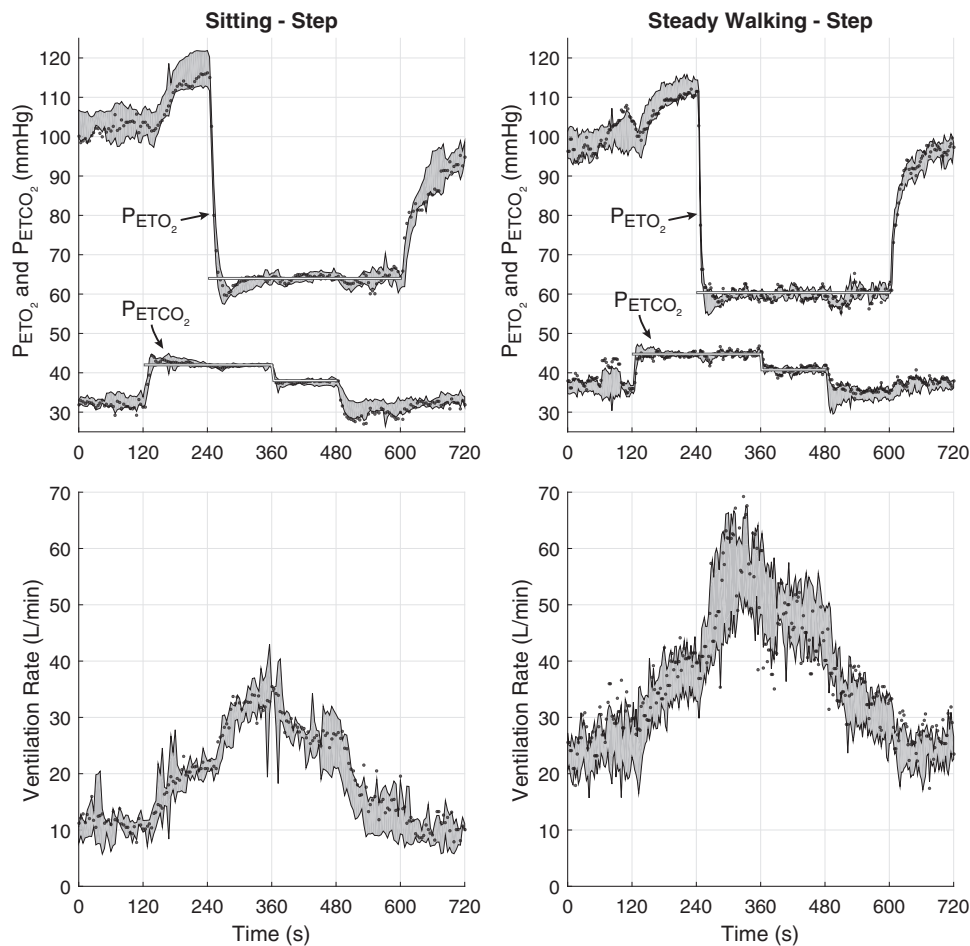


Fig. 2. End-tidal values and minute expired ventilation during end-tidal step protocol while sitting (*trial 1*) and walking at 1.25 m/s (*trial 2*). Raw breath-by-breath data from an example subject is indicated by black circles. White lines indicated reference end-tidal values. The gray area represents the 95% confidence interval on the group mean data.

control is turned on, inducing a 40-mmHg drop in P_{ETO_2} and a sudden increase in \dot{V}_E . The timing and error metrics showed significant effects of trial type only for time delay ($P = 0.015$) and mean error ($P = 0.014$). However, post hoc comparisons found no significant difference between individual trials.

Step P_{ETO_2} Performance (Trials 1–3)

For all trials where step changes in P_{ETCO_2} were controlled, measured end-tidal values responded with an average time delay of 0.6 ± 0.5 breaths and an average rise time of 3.8 ± 0.8 breaths (Table 3). P_{ETO_2} tended to overshoot reference values by 3.0 ± 2.6 mmHg (7.3% overshoot) before settling within 5.0 ± 2.6 breaths. The average standard deviation for P_{ETO_2} after the rise period was 1.8 ± 0.4 mmHg, corresponding to a $2.9 \pm 0.7\%$ coefficient of variation. The mean value after the rise period was 0.3 ± 0.8 mmHg above the reference values, where this error was not significantly different from zero ($P = 0.24$). These metrics include the time period where P_{ETCO_2} suddenly steps from +7 to +4 and where P_{ETCO_2} control is later turned off, events which both induced sudden drops in \dot{V}_E . These timing and error metrics showed significant effects of trial type only for time delay ($P = 0.026$) and overshoot ($P = 0.017$). Post hoc comparisons found significant difference between individual trials only for overshoot (*trials 3 and 5*, $P = 0.019$).

Chirp End-tidal Performance (Trial 4)

Chirp signal time courses demonstrate frequency dependence of end-tidal control performance (Fig. 4). The system bandwidth, indicated by the signal frequency at which the system gain falls below -3 dB, occurred at 0.066 ± 0.003 and 0.053 ± 0.009 Hz for P_{ETCO_2} and P_{ETO_2} , respectively. A more conservative measure of bandwidth, where the gain falls below -0.92 dB (10% error), occurred at 0.062 ± 0.006 and 0.025 ± 0.006 Hz for P_{ETCO_2} and P_{ETO_2} , respectively. A second measure of control performance is indicated by the signal frequency at which phase lag exceeds 45° , which we found to occur at 0.026 ± 0.009 and 0.020 ± 0.002 Hz for P_{ETCO_2} and P_{ETO_2} , respectively. A 45° delay at these frequencies corresponds to a time delay of 5.1 s and 6.3 s for P_{ETCO_2} and P_{ETO_2} , respectively. Root mean squares error between reference and measured values at frequencies less than the respective 45° phase lag frequencies were 1.4 ± 0.3 and 10.7 ± 3.3 mmHg for P_{ETCO_2} and P_{ETO_2} , respectively.

DISCUSSION

We successfully designed and validated a generalized active end-tidal forcing system that removed the need for manual tuning and control heuristics. This design allows for accurate control of gases along spontaneous and complicated time courses, including under nonsteady metabolic expenditure con-

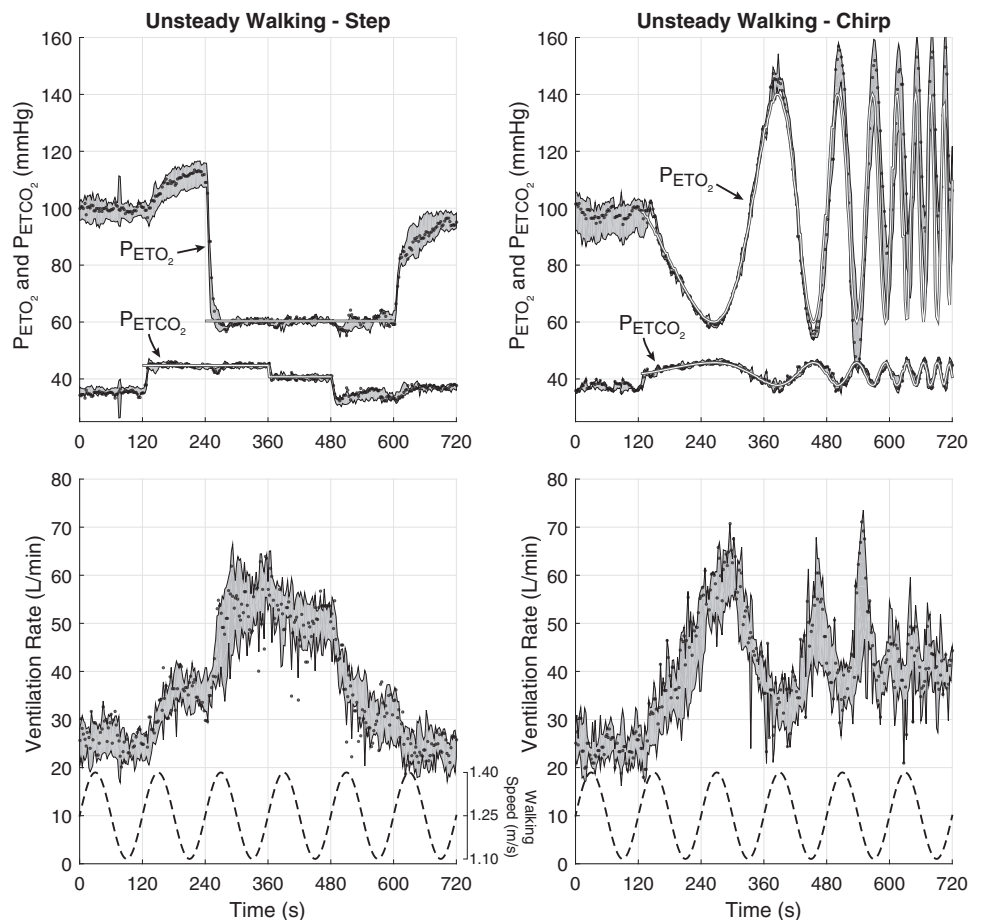


Fig. 3. End-tidal values and minute expired ventilation during nonsteady state walking for the end-tidal step protocol (trial 3) and chirp protocol (trial 4). Raw breath-by-breath data from an example subject is indicated by black circles. White lines indicated reference end-tidal values. The gray area represents the 95% confidence interval on the group mean data.

ditions. These findings suggest that end-tidal controllers will benefit by using models to account for the dynamic nature of the human cardiopulmonary system. The controller handles both the initial control and maintenance of end-tidal values by complementary processes (Fig. 5). The initial control is predominantly accomplished with feedforward control, which plans adjustments in the inspired gas concentrations to affect sudden change in the fast changing gas compartments (lung and arterial blood). The maintenance of end-tidal values over longer time scales is largely accomplished with ventilation compensation and feedback control. The former compensates for \dot{V}_E adaptations in response to end-tidal control and the latter accommodates filling and emptying of gases in body tissue, changes in metabolic rate, and errors associated with the other controllers.

While quantitative comparisons are difficult, our system performance is similar to two other ETF systems, dynamic end-tidal forcing and prospective end-tidal targeting, for step changes in end-tidal values during resting conditions. The former system adapts the inspired concentrations using feedback control (control signals based on measured end-tidal errors) (13, 20), while the latter system estimates required inspired values and passively corrects end-tidal errors due to \dot{V}_E using a novel valve design worn at the mouth (22). Similar to these systems, step change performance during sitting (trial 1) demonstrates precise and independent control of P_{ETCO_2} and P_{ETO_2} in steady-state despite two- to threefold changes in \dot{V}_E , maintaining values with an absolute error of <0.5 mmHg and standard deviation less than 1 and 2 mmHg for P_{ETCO_2} and P_{ETO_2} , respectively (13, 22). Further comparisons are difficult

Table 2. Summary of performance parameters for control of P_{ETCO_2}

	Sitting Step	Steady Walk Step	Nonsteady Walk Step
Time delay, breaths	0.2 (0.4)	0.4 (0.5)	1.0 (0.0)
Rise time, breaths	2.3 (0.5)	2.3 (0.8)	2.8 (0.7)
Settling time, breaths	11.6 (5.7)	7.9 (5.4)	5.2 (4.3)
Overshoot, mmHg	1.49 (0.34)	1.01 (0.83)	0.49 (0.74)
SS error, mmHg	-0.07 (0.11)	0.03 (0.07)	0.32 (0.27)
SS variability, mmHg	0.69 (0.19)	0.79 (0.15)	0.82 (0.04)

Values are presented as mean \pm SD. SS, steady state.

Table 3. Summary of performance parameters for control of P_{ETO_2}

	Sitting Step	Steady Walk Step	Nonsteady Walk Step
Time delay, breaths	1.0 (0.0)	0.2 (0.4)	0.6 (0.5)
Rise time, breaths	4.0 (0.8)	3.5 (0.7)	3.9 (0.7)
Settling time, breaths	6.3 (2.5)	4.8 (3.0)	3.9 (0.7)
Overshoot, mmHg	5.29 (1.38)	2.84 (2.42)	0.91 (1.10)
SS error, mmHg	0.43 (0.17)	-0.07 (1.20)	0.40 (0.29)
SS variability, mmHg	1.89 (0.27)	1.89 (0.52)	1.52 (0.14)

Values are presented as mean \pm SD.

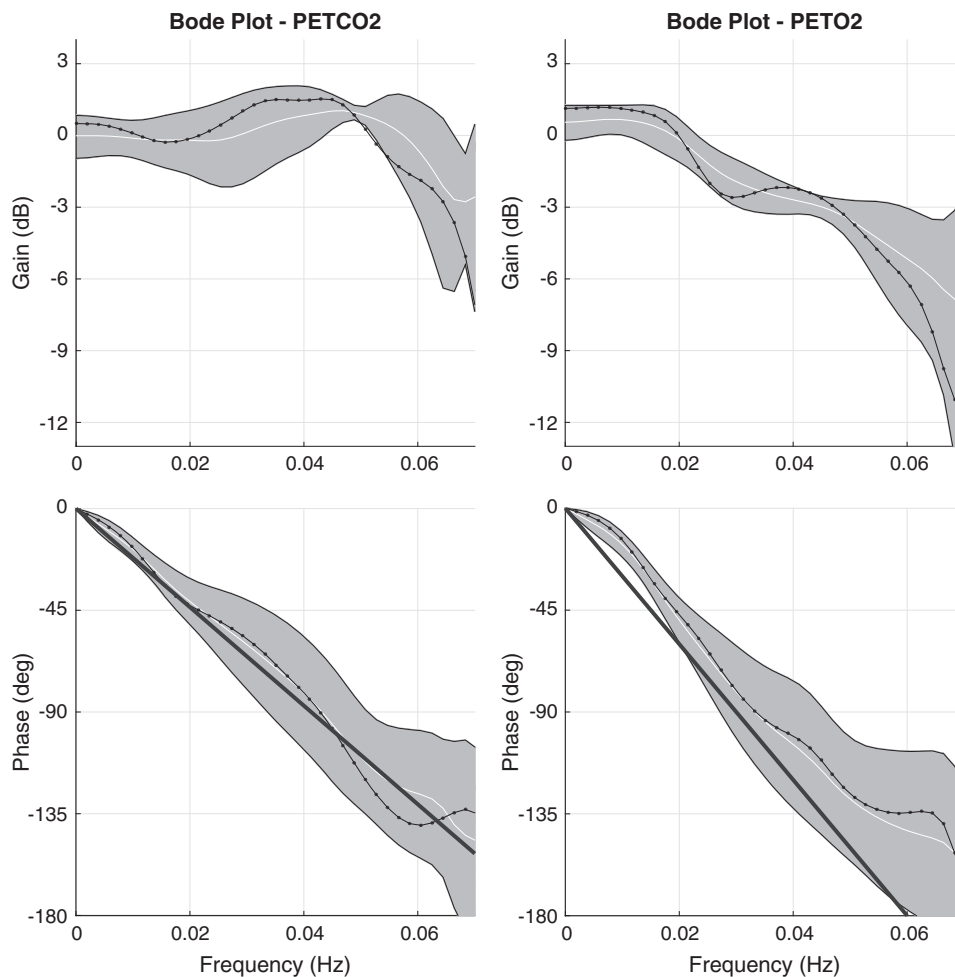


Fig. 4. Bode plot, system gain, and phase as a function of reference signal frequency content, based on chirp end-tidal perturbations of PETCO_2 and PETO_2 . Gain and phase values from an example subject are indicated by black circles. Gray areas represent the 95% confidence interval on the group mean data. The thick dark lines indicated theoretical phase given a fixed delay of 3.0 and 4.4 breaths for PETCO_2 and PETO_2 , respectively, equivalent to the average time delay plus rise time measured during the step performance walking trials.

because timing performance metrics have not previously been quantified in detail. Here, we have provided a quantitative analysis of ETF system performance metrics not typically reported in ETF validations, such as time delay, rise time, overshoot, and settling time. These parameters roughly quantify performance of the individual components of the ETF system. The time delay is associated with delays in delivering controlled air to the subject due to end-tidal measurement delays and gas transit. Rise time and overshoot values may largely be attributed to errors in the timing and amplitude of the feedforward control signal, respectively. Settling time reflects errors in feedback control and ventilation compensation. These additional parameters should be reported in future ETF system validations, as they directly establish the limits of end-tidal control.

While step changes during sitting demonstrated similar performance to previous systems, our system was more broadly designed to handle the requirements of nonsteady exercise and nonprescribed time courses. Other groups have used their own heuristics to speed up transitions during a step change with subjects at rest. For example, Slessarev et al. used an overshooting technique that set the reference value larger than desired for two to three breaths and then returned the reference to the desired value (14, 19–22). Similarly, Koehle et al. delivered “bolus” mixtures for three breaths based on the amount of gas needed to change blood concentration before

enacting feedback control (9, 11–13). Our controller also effectively delivers a bolus to speed step transitions, but this behavior naturally emerges out of the cardiopulmonary model based controller. This same controller will automatically provide the correct inspired gas concentrations for any reference end-tidal time course. In theory, this controller could be implemented in other active ETF systems as a software update. Additionally, step change performance during steady walking (*trial 2*) verifies control of independent step changes during conditions with higher metabolic rate and minute ventilation and higher variability, conditions not previously tested in other ETF systems.

Our methods also produce consistent controller performance in more difficult control conditions. Step change performance during sinusoidally varying treadmill speed (*trial 3*) verifies generality of the system and ability to control during nonsteady metabolic expenditure. Chirp change performance (*trial 4*) demonstrates end-tidal control along time courses that are more complicated than step changes and that mimic profiles that limit the success of heuristic based approaches. Both trials also demonstrate precise control despite higher \dot{V}_E variability. Note that although the chirp signal is prescribed in advance, the control system was given no advanced knowledge of the signal (20) and, given its dynamic nature, is meant to mimic the conditions that could possibly occur if end-tidal refer-

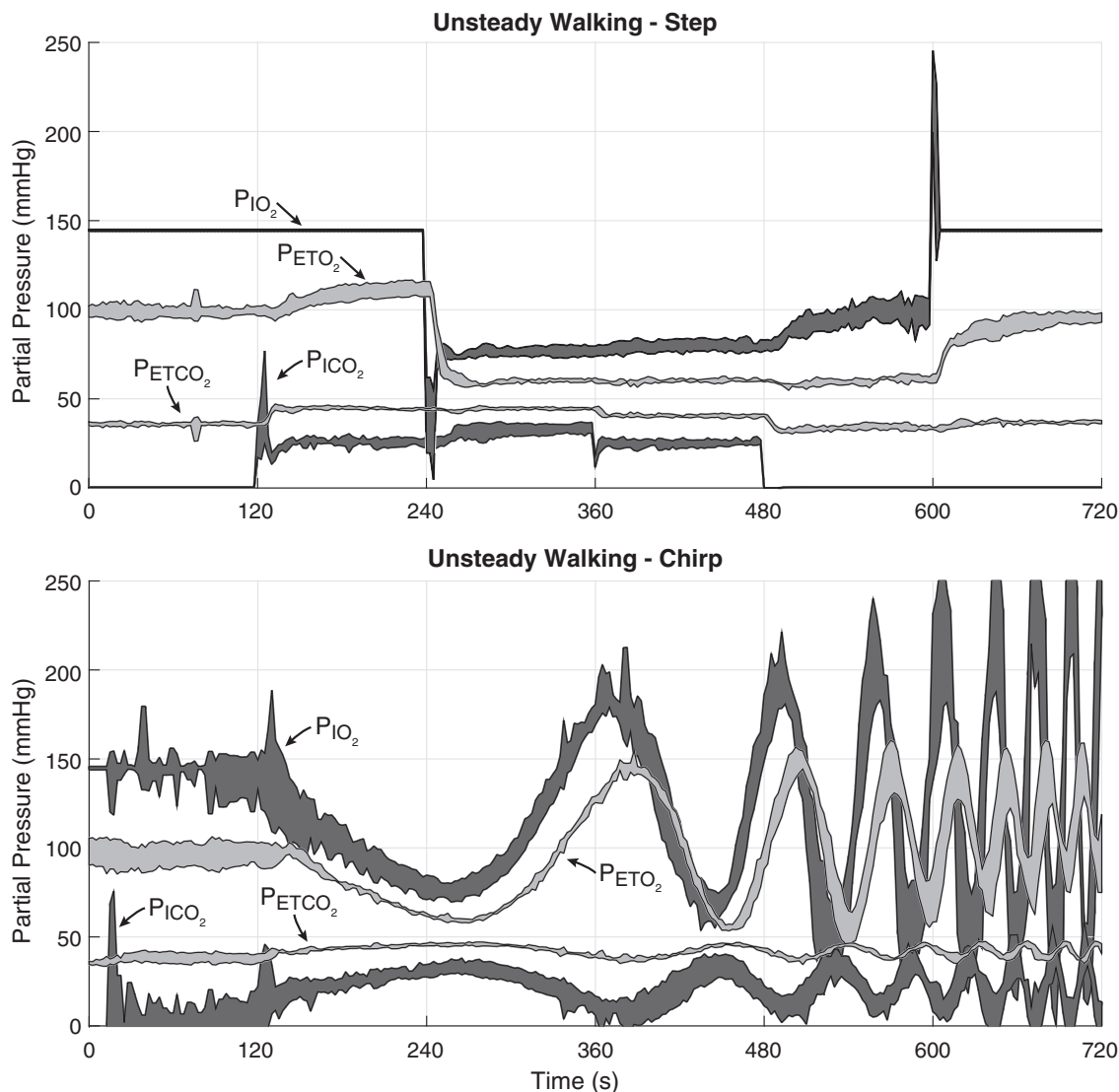


Fig. 5. End-tidal values and inspired values during end-tidal step protocol for nonsteady-state walking (trial 3) and chirp protocol (trial 4). The light gray area represents the 95% confidence interval on the group mean end-tidal value data (replotted from Fig. 3). The dark gray area represents the 95% confidence interval on the group mean inspired partial pressure data planned by the control system.

ence values were chosen in real-time based on measured respiratory, metabolic, or biomechanical variables.

The chirp signal findings also quantified controller bandwidth. Using system gain as a performance metric, we found that the controller achieved a bandwidth (i.e., gain within ± 3 dB) beyond 1/20 Hz for both PETCO₂ and PETO₂ control. This bandwidth is equivalent to completing one sinusoidal cycle in 20 s. A practical rule of thumb for feedback control systems is that the sampling frequency (in our case, the breathing frequency) should be 10 times greater than the controller bandwidth (27). Since we measured a maximum breathing frequency of $\sim 1/2$ Hz, our controller bandwidth covers the theoretically practical range. The measured gain-based bandwidths of 0.066 and 0.053 Hz for PETCO₂ and PETO₂ control, respectively, indicated that our ETF system can be expected to accurately control end-tidal values along any preplanned time course that contains frequency content within these ranges, albeit with a half breath delay. This bandwidth limitation predicts that measured end-tidal values

would demonstrate a 2.8 and 3.5 breath rise time in response to a step change in reference values. These values are very close to the measured rise times from the step change trials (Tables 2 and 3), highlighting that controller bandwidth dictates the early step responses. However, system phase may be a more useful performance metric for end-tidal time courses planned in real-time because phase lag limits the correlation between reference and measured end-tidal values. By this criterion the bandwidth is limited to 0.026 and 0.020 Hz for PETCO₂ and PETO₂, respectively, or about half the tested frequency range. The phase lag appears to be significantly explained by the time delays plus rise times of 3.0 and 4.4 breaths, respectively, measured from the step change trials (Fig. 4). Future technical advancements, such as reducing the delay in measuring end-tidal values or improving the accuracy of the model used for feedforward control planning, could significantly increase the phase-based bandwidth (if these delays were halved, phase-based bandwidth would double).

The experimental methods are subject to several limitations. First, use of a facemask and nonbreathing valves introduced significant dead space into the breathing circuit and therefore limited the amount of new air that can be delivered at each breath. Replacing the facemask with a mouthpiece and using smaller valves could minimize dead space but subjects generally found these options uncomfortable. Also, when using a facemask, care must be taken to ensure proper fitting to avoid leaks. Second, limitations in the control system clock speed (240 Hz) potentially reduced accuracy of gas delivery through the solenoid valves since delivered volume is controlled by the valve open duration. For example, a 2-ms error in oxygen valve timing (possible at 240 Hz) would result in an error of 1.4 ml of O₂ or 1.5 mmHg for control around normal breathing. Future iterations of the ETF system could increase delivery accuracy by controlling valve timing at a higher clock speed or by replacing solenoid valves with mass flow controllers, which provide a continuous flow rate as a function of a command voltage. System delays also significantly limit feedback correction of short term end-tidal variations, induced by noise-like breath-by-breath adjustments in \dot{V}_E . While our system minimized the delay in controlled air delivery to ~0.7 s after the end of exhalation, this delay represents roughly half an inhalation period and therefore significantly limits feedback correction of short-term end-tidal errors.

Our ETF system also assumes that end-tidal gas values may be used as a proxy for the more difficult to measure arterial blood gas values. However, the difference between these values varies with ventilation rate associated changes to the dead space/tidal volume ratio (V_D/V_T) (11, 15, 25). Also this assumption may not hold for subjects with lung disease or heart failure. Since ventilation rate, and thus V_D/V_T , adaptations lag behind end-tidal changes, relatively fast end-tidal perturbations (e.g., initial portion of a step signal or high-frequency portion of a chirp signal) are expected to produce a 1:1 change in arterial values in healthy subjects, albeit with an absolute difference based on the instantaneous V_D/V_T . Slower end-tidal perturbations that induce significant minute ventilation adaptations would perturb arterial values but to a significantly lesser degree. End-tidal values have been shown to accurately represent arterial values when using a prospective end-tidal targeting or passive feedback system (10). This system uses a novel breathing apparatus to reduce variations of respiratory gases within the lung and improve matching between end-tidal and arterial gas values. Future systems could ideally combine the benefits of our controller with the passive feedback system's breathing apparatus to improve end-tidal and arterial coupling.

Since our ETF control system was based on a specific model of the human cardiopulmonary system (see APPENDIX), successful end-tidal control provides insight into the applicability of that model. Specifically, we used a two compartment model of the cardiorespiratory system, where the lungs and body tissue are modeled as separate, fixed-volume systems receiving continuous inspiratory and expiratory flows and connected by continuously circulating arterial and venous blood (12). These "gill-type" models do not account for spatial and temporal variations of gas levels in the lung and body tissue due to the pulsatory nature of ventilation and cardiac output. This simplification is thought to explain why such models do not predict the dissociation of end-tidal and arterial values or account for variations in dead space (8, 11). One direct test of this issue is

whether a controller based on this model allows precise control of end-tidal values. The success in controlling steady and nonsteady end-tidal time courses during a variety of metabolic expenditure conditions suggests that this model does serve as a valid model of cardiorespiratory dynamics, at least for the purpose of planning controller parameters.

Generalized end-tidal control is necessary for future studies that require control during nonsteady conditions and for which the reference values cannot be planned ahead of time. One potential application is the control of end-tidal values during nonsteady exercise for the purposes of better estimating the role of blood gases in the hyperpnea response to sudden onset of exercise. A second application involves measuring cerebrovascular reactivity to CO₂, which is often used as a noninvasive measure for cerebrovascular function. When measuring cerebral blood flow it is important to control other, confounding, vasoactive stimuli, such as O₂ in the case of a CO₂ perturbation. This is a particular challenge when investigating responses to hypocapnia because the subject must voluntarily hyperventilate to expel metabolically produced CO₂, thereby reducing P_{ETCO_2} but also forcing P_{ETO_2} to rise when uncontrolled.

Finally, this device could allow us to investigate the potential role of blood gas chemoreceptors in sensing ongoing metabolic cost. Our recent work has demonstrated that the nervous system can compute motor commands that minimize energetic cost (21). For the nervous system to optimize energetic cost, it must presumably sense the metabolic cost of ongoing movement. Candidate sensory systems include those that are sensitive to signals related to metabolic cost, and have a known role in controlling aspects of respiratory or locomotion physiology. Since a decreased concentration of O₂ and simultaneous increased concentration of CO₂ in the blood reflects an increase in net metabolism, blood gas chemoreceptors that measure these changes are one candidate sensory system. This experiment would disassociate actual and perceived metabolic rate by stimulating the chemoreceptors based on the continuously measured properties of the subject's movement, such as step frequency, and thus simulate for these sensors a novel relationship between metabolic cost and movement. If subjects adapt movement patterns to reduce perceived cost, this would be evidence that blood gas chemoreceptors signal metabolic cost for optimizing movement. For example, P_{ETCO_2} could be controlled to negatively correlate with measured step frequency to determine if subjects increase preferred step frequency to reduce P_{ETCO_2} , and thus sensed energy expenditure. Such an experiment specifically requires nonprescribed end-tidal reference signals that vary in real time as a function of movement parameters.

APPENDIX

Cardiopulmonary Model

Establishing a model of the system, or plant, to be controlled is a critical phase of control system design. The plant model mathematically describes how the plant's outputs vary in response to changes in its inputs. Our goal was to develop a control system for prescribing the end-tidal partial pressures of carbon dioxide and oxygen, P_{ETCO_2} and P_{ETO_2} , in human subjects. In this case, our plant is the human respiratory system and the experimentally controllable inputs to the system are the

inspired partial pressures of carbon dioxide and oxygen, P_{iCO_2} and P_{iO_2} . Noncontrolled variables are the metabolic rate of oxygen use and carbon dioxide production, \dot{V}_{CO_2} and \dot{V}_{O_2} , and the minute alveolar ventilation, \dot{V}_A , which can independently affect end-tidal values. End-tidal perturbations due to changes in these variables are treated as disturbances to be rejected by the control system. This supplement describes model development and controller design for P_{ETCO_2} control, assuming equivalence of end-tidal and arterial values. A similar process informed P_{ETO_2} controller design but is not presented in detail here.

We modeled the cardiorespiratory plant based on established differential equations describing transfer of respiratory gases in the lung and body tissues. Specifically, we used a two compartment model of the cardiorespiratory system, where the lungs and body tissue are modeled as separate, fixed-volume systems connected by the circulating arterial and venous blood (12). This model further uses blood gas dissociation curves and simplifying assumptions to convert the lung and body tissue equations into common units and develop a single equation, or transfer function, relating inspired gas partial pressures to arterial values. Khoo et al. used this model to derive a transfer function relating arterial gas values to changes in \dot{V}_A . Here, we derive a transfer function relating arterial gas values to change in inspired gas values. Finally, we designed control system parameters directly from the transfer function based on standard design rules. While the model assumptions and simplifications do reduce the accuracy of arterial gas predictions, a perfect model is not necessary to achieve successful control as feedback control is particularly suited to compensate for control errors induced by model inaccuracies.

Lung compartment. The model of the lung compartment for CO_2 (Eq. A1) describes a mass balance for CO_2 within a fixed-volume lung system, where the summation of CO_2 transfer into the lung by the circulatory system and out of the lung by the ventilatory system determines the rate of change of the CO_2 concentration in the lung.

$$V_{ACO_2} \frac{dF_{ACO_2}}{dt} = \frac{863}{P_{amb} - 47} \dot{Q}_p (C\bar{V}CO_2 - Ca_{CO_2}) + \dot{V}_A (F_{iCO_2} - F_{ACO_2}) \quad (A1)$$

Here, V_{ACO_2} is the functional storage volume of the lung with respect to CO_2 , \dot{Q}_p is the pulmonary blood flow rate, $C\bar{V}CO_2$ and Ca_{CO_2} are concentrations of CO_2 in the mixed venous and arterial blood, \dot{V}_A is the minute alveolar ventilation, and F_{iCO_2} and F_{ACO_2} are the fractional concentrations of CO_2 in the inspired and alveolar air mixtures. See Tables A1 and A2 for description of variable and parameter units and typical values. The term $863/(P_{amb} - 47)$ is a conversion factor (units of l_{BTPS}/l_{STPD}) that accounts for the fact that V_{ACO_2} and \dot{V}_A are measured under BTPS (body temperature and pressure, saturated) conditions while $C\bar{V}CO_2$ and Ca_{CO_2} are measured under STPD (standard temperature and pressure, dry) conditions. Here, P_{amb} is ambient pressure and 47 is the vapor pressure of water at body temperature in units of mmHg. These equations are also referred to as “gill models” of respiration because they assume that ventilation and perfu-

Table A1. Model variables

Symbol	Description	Units
\dot{V}_E	Minute expired ventilation	l/s
\dot{V}_A	Minute alveolar ventilation	l/s
\dot{Q}_p	Pulmonary blood flow rate	l/s
\dot{Q}_s	Systemic blood flow rate	l/s
Q	Cardiac output	l/s
F_{ACO_2}, F_{AO_2}	Fractional concentration of CO_2 and O_2 in the alveolar air	Dimensionless
F_{iCO_2}, F_{iO_2}	Fractional concentration of CO_2 and O_2 in the inspired air	Dimensionless
F_{aCO_2}, F_{aO_2}	Fractional concentration of CO_2 and O_2 in the arterial blood	Dimensionless
P_{ETCO_2}, P_{ETO_2}	End-tidal partial pressure of carbon dioxide and oxygen	mmHg
P_{ACO_2}, P_{AO_2}	Alveolar partial pressure of carbon dioxide and oxygen	mmHg
P_{aCO_2}, P_{aO_2}	Arterial partial pressure of carbon dioxide and oxygen	mmHg
$P\bar{V}CO_2, P\bar{V}O_2$	Venous partial pressure of carbon dioxide and oxygen	mmHg
P_{iCO_2}, P_{iO_2}	Inspired partial pressure of carbon dioxide and oxygen	mmHg
$C\bar{V}CO_2, C\bar{V}O_2$	Concentration of CO_2 and O_2 in the venous blood	ml gas/ml blood
Ca_{CO_2}, Ca_{O_2}	Concentration of CO_2 and O_2 in the arterial blood	ml gas/ml blood
$\dot{V}_{CO_2}, \dot{V}_{O_2}$	Metabolic rate of carbon dioxide production and oxygen consumption	l/s

sion of the lung are not tidal and pulsatile processes, respectively, but instead continuous processes (8).

Body tissue compartment. The model of the body tissue compartment for CO_2 (Eq. A2) describes a mass balance for CO_2 within a fixed-volume body tissue system.

$$V_{T_{CO_2}} \frac{dC_{T_{CO_2}}}{dt} = \dot{Q}_s (Ca_{CO_2} - C\bar{V}CO_2) + \dot{V}_{CO_2} \quad (A2)$$

Here, $V_{T_{CO_2}}$ is the functional storage volume of the body tissues with respect to CO_2 , $C_{T_{CO_2}}$ is the concentration of CO_2 in the tissue compartment, \dot{Q}_s is the systemic blood flow rate, and \dot{V}_{CO_2} is the rate of metabolic CO_2 production.

Dissociation curves. The dissociation curve for CO_2 relates blood gas concentrations to blood gas partial pressures and may be approximated by a linear function (16)

$$Ca_{CO_2} = K_{CO_2} Pa_{CO_2} + k_{CO_2} \quad (A3)$$

where K_{CO_2} (1/mmHg) and k_{CO_2} (dimensionless) are the slope and offset of the dissociation curve, respectively, and Pa_{CO_2} is the arterial partial pressure of CO_2 . This dissociation relation is also assumed to apply to venous blood and body tissues.

Simplifying assumptions. Further simplification of the above equations is necessary to limit the number of independent, time-varying parameters and to allow the differential equations to be solved for Pa_{CO_2} as a function of changes in P_{iCO_2} (12).

Assumption 1: blood flow is in steady state and therefore the rate of pulmonary blood flow \dot{Q}_p , system blood flow \dot{Q}_s , and cardiac output Q are all equal ($\dot{Q}_p = \dot{Q}_s = Q$).

Assumption 2: diffusion of gases between the pulmonary capillaries and the alveolar gas is rapid relative to respiratory frequency and therefore the gas fractions of arterial and alve-

Table A2. Model parameters

Symbol	Description	Values	Reference
V_{ACO_2}, V_{AO_2}	Storage volume of the lung compartment with respect to CO ₂ and O ₂ given a measured lung volume of 2.5 liters	3.2, 2.5 L	(12)
$V_{T_{CO_2}}, V_{T_{O_2}}$	Storage volume of the body tissues with respect to CO ₂ and O ₂ given a measured lung volume of 2.5 liters	15.0, 6.0 L	(16)
P_{amb} K_{CO_2}	Ambient air pressure Dissociation curved parameters for CO ₂	760 mmHg 0.0065 mmHg ⁻¹	(16)
K_{O_2}	Dissociation curved parameters for O ₂	0.00025 mmHg ⁻¹ (70 < Pa _{O₂}) 0.00067 mmHg ⁻¹ (55 < Pa _{O₂} < 70) 0.00211 mmHg ⁻¹ (35 < Pa _{O₂} < 55)	(16)

olar blood gases are in equilibrium (e.g., $F_{ACO_2} = F_{aCO_2}$ for CO₂).

Assumption 3: diffusion of gases between the systemic capillaries and the body tissues is rapid relative to other modeled transport dynamics and therefore the partial pressures of venous and body tissue blood gases are in equilibrium (e.g., $C_{T_{CO_2}} = C_{V_{CO_2}}$ for CO₂).

Substitution 1: fractional concentrations of gas can be expressed as partial pressures, where $P_{ACO_2} = F_{ACO_2} (P_{amb} - 47)$ for alveolar CO₂ and where P_{ACO_2} is the alveolar partial pressure of CO₂.

Simplified differential equations. Equations A1 and A2 can be simplified by substituting in the dissociation equation (Eq. A3) and simplifying assumptions to yield lung and tissue equations that share PaCO₂ and P \bar{V}_{CO_2} as common, time-dependent variables.

$$V_{ACO_2} \frac{dPa_{CO_2}}{dt} = 863\dot{Q}K_{CO_2}(P\bar{V}_{CO_2} - Pa_{CO_2}) + \dot{V}_A(P_{I_{CO_2}} - Pa_{CO_2}) \quad (A4)$$

$$V_{T_{CO_2}}K_{CO_2} \frac{dP\bar{V}_{CO_2}}{dt} = \dot{Q}K_{CO_2}(Pa_{CO_2} - P\bar{V}_{CO_2}) + \dot{V}_{CO_2} \quad (A5)$$

Laplace formulation of equations. We then take the Laplace transform of Eqs. A4 and A5 to convert them from differential equations to algebraic equations for PaCO₂, where s is the Laplace variable.

$$(V_{ACO_2}s + 863\dot{Q}K_{CO_2} + \dot{V}_A)Pa_{CO_2}(s) - 863\dot{Q}K_{CO_2}P\bar{V}_{CO_2}(s) = \dot{V}_AP_{I_{CO_2}}(s) \quad (A6)$$

$$P\bar{V}_{CO_2}(s) = \left(\frac{\dot{Q}K_{CO_2}}{V_{T_{CO_2}}K_{CO_2}s + \dot{Q}K_{CO_2}} \right) Pa_{CO_2}(s) + \left(\frac{1}{V_{T_{CO_2}}K_{CO_2}s + \dot{Q}K_{CO_2}} \right) \dot{V}_{CO_2}(s) \quad (A7)$$

After substituting Eq. A7 into Eq. A6, and solving for PaCO₂(s), we arrive at a general equation that describes how changes in PaCO₂(s) vary as a function of changes in P \bar{V}_{CO_2} and \dot{V}_{CO_2} .

$$Pa_{CO_2}(s) = \frac{\left(\frac{\dot{V}_A}{V_{ACO_2}} \right) P_{I_{CO_2}}(s) + \left(\frac{863}{V_{ACO_2}} \right) \left(\frac{1}{(V_{T_{CO_2}}/\dot{Q})s + 1} \right) \dot{V}_{CO_2}(s)}{s + \frac{863\dot{Q}K_{CO_2}}{V_{ACO_2}} + \frac{\dot{V}_A}{V_{ACO_2}} - \left(\frac{863\dot{Q}K_{CO_2}}{V_{ACO_2}} \right) \left(\frac{1}{(V_{T_{CO_2}}/\dot{Q})s + 1} \right)} \quad (A8)$$

Although Eq. A8 has two parallel inputs (two additive terms in the numerator), our purpose is to develop a transfer function describing only the input/output relationship between P \bar{V}_{CO_2} and PaCO₂. When formulating how a relative to baseline change in P \bar{V}_{CO_2} induces a relative change in PaCO₂, the right side of the numerator does not contribute and can be mathematically neglected. While \dot{V}_A and \dot{Q} may also be considered inputs to the system (as in Khoo), they will be treated as model parameters because they nonlinearly couple to P \bar{V}_{CO_2} .

Equation A8 may be further simplified by grouping of model parameters to represent physiologically relevant mean residence times associated with filling a fixed volume at a constant flowrate,

$$T_1 = \frac{V_{ACO_2}}{863\dot{Q}K_{CO_2}}, T_2 = \frac{V_{ACO_2}}{\dot{V}_A}, T_3 = \frac{V_{T_{CO_2}}}{\dot{Q}} \quad (A9)$$

where T_1 , T_2 , and T_3 represent mean residence times associated with blood perfusion of the lung, air perfusion of the lung, and blood perfusion of the body tissue, respectively.

Plant model transfer function equation. We derived a final transfer function for the plant P(s) describing the relative arterial blood gas response to changes in inspired gas by

solving Eq. A8 for $\frac{Pa_{CO_2}(s)}{P_{I_{CO_2}}(s)}$ and substituting in time parameters from Eq. A9.

$$P(s) = \frac{Pa_{CO_2}(s)}{P_{I_{CO_2}}(s)} = \frac{T_1(T_3s + 1)}{T_1T_2T_3s^2 + (T_1T_2 + T_1T_3 + T_2T_3)s + T_1} \quad (A10)$$

This final transfer function then varies with subject specific volume parameters (V_{ACO_2} , $V_{T_{CO_2}}$) and time dependent parameters (\dot{V}_A , \dot{Q}). These timing parameters are dynamically updated at each breath based on a five breath running median filter for \dot{V}_A and estimation of \dot{Q} (see *Measurement of Model Parameters*). The arterial response is then estimated by multiplying the plant model by the inspired gas input.

Control System Design

The control system first uses a combination of feedforward and feedback controller functions to maintain end-tidal values along a desired time course. The design of these controller

functions are based directly on the plant model (Eq. A10). The system takes the form

$$P_{iCO_2_control} = f_{FF}(Pa_{CO_2,desired}) + f_{FB}(Pa_{CO_2,error}) \quad (A11)$$

where $P_{iCO_2_control}$ is the inspiratory partial pressure of CO_2 planned by the controller for the subsequent breath; f_{FB} is the feedback controller that varies as a function of the error, or difference, between desired and measured arterial values; and f_{FF} is the feedforward controller that varies as a function of desired values. In the Laplace domain, the controller takes the form

$$P_{iCO_2_control}(s) = FF(s)Pa_{CO_2,desired}(s) + FB(s)Pa_{CO_2,error}(s) \quad (A12)$$

where the feedforward and feedback controller functions are parameterized based on the timing parameters (Eq. A9). While measured ventilation changes then adjust the controller parameters at each breath, these adjustments do not specifically compensate for the direct perturbation of arterial values by \dot{V}_A . Feedback control can compensate for these arterial errors; however, we found that performance could be improved further by correcting the controller planned inspired gases by a ventilation compensation function,

$$P_{iCO_2_corrected} = f_{VC}(P_{iCO_2_control}, \dot{V}_A) \quad (A13)$$

where f_{VC} is the ventilation compensation function and where this function directly accounts for end-tidal perturbations caused by changes in measured \dot{V}_A (see *Measurement of Model Parameters*).

Feedforward controller. The feedforward controller plans inspired gas values based only on desired arterial time courses and controller design is equivalent to using an inverse of the plant transfer function.

$$P^{-1}(s) = \frac{1}{P(s)} = \frac{T_1T_2T_3s^2 + (T_1T_2 + T_1T_3 + T_2T_3)s + T_1}{T_1(T_3s + 1)} \quad (A14)$$

However, since $P(s)$ is a proper transfer function (the degree of the denominator is greater than the degree of the numerator), inversion results in a function that grows unbounded at high frequencies, such as would be present for step change in desired values. We therefore multiplied the inverted system by a low pass filter with filter time constant τ chosen to equal the smallest timing parameter (T_1) to reduce high-frequency sensitivity while minimizing distortion of the plant dynamics. For implementation in the end-tidal controller, this continuous feedforward model was converted to a discrete model with a one breath sampling period.

$$FF(s) = \frac{1}{P(s)} \frac{1}{\tau s + 1} = \frac{T_1T_2T_3s^2 + (T_1T_2 + T_1T_3 + T_2T_3)s + T_1}{T_1(T_3s + 1)(T_1s + 1)} \quad (A15)$$

Since the feedforward contributions to the control system are planned by running the desired end-tidal time courses through an approximate inverse of the plant dynamics, the accuracy of this control is dependent on the degree to which the plant

model and associated parameters reflect the actual cardiopulmonary system of each subject. If the plant model is perfectly accurate, then feedforward control is sufficient and there is little need for feedback control. In practice, inaccuracies in model assumptions and simplifications, parameter estimation, and controlled gas delivery limit the effectiveness of feedforward control. While breath by breath measures of \dot{V}_A and estimation of \dot{Q} update the plant model, and therefore the sensitivity of arterial values to changes in inspired values, the model also neglects the direct effect that \dot{V}_A , \dot{Q} , and V_{CO_2} inputs have on arterial values. The feedforward controller is then most accurate over the short time period (<5 breaths) after a change in desired value, when the unmodeled perturbations are relatively constant.

Feedback controller. The feedback controller plans inspired gas values based on the error between desired and measured arterial values and takes the form of a standard proportional-integral (PI) controller

$$FB(s) = K_P + K_I/s \quad (A16)$$

where K_P and K_I are the proportional and integral gains, respectively.

To parameterize the feedback gains as a function of model parameters using standard tuning rules, we further simplified the plant model (Eq. A10) to a first order system with time delay. It is common practice to reduce higher order systems to simplify feedback controller design in cases where some system dynamics operate at a much slower time scale than others. In this case, the feedback controller is designed based on the reduced system, which retains the fast dynamics. Such a design faces relatively little loss in controller performance because a controller designed to regulate the faster time scale processes is sufficiently fast to regulate the slower time scale processes. The timing parameter T_3 is approximately five times greater than T_2 and 30 times greater than T_1 , reflecting that fact that changes in the body tissue CO_2 levels change more slowly than in the lung. We therefore simplified Eq. A10 with the assumption that $T_3 \gg T_2, T_1$, equivalent to assuming P_{VCO_2} is constant. The reduced model $P^*(s)$ takes the form,

$$P^*(s) = \frac{(T_1/(T_1 + T_2))}{((T_1T_2)/(T_1 + T_2))s + 1} \quad (A17)$$

and served the purpose of designing the feedback gains. This derived model assumes no time delay between changes in inspired air concentration and changes in arterial concentration. In practice, delivery of controlled air to the subject is limited by sensor delay, transit delay, and filtering delay (see MATERIALS AND METHODS) and we estimated this delay to be approximately one breath in pilot experiments.

We chose these gains based on plant model dynamics using standard design rules which seek a balance between fast rejection of errors and closed-loop stability. Using the reduced model allows application of the second method of Zeigler-Nichol's PI tuning (30). For a generic first order system with time delay, $G(s)$, the proportional and integral gains are a direct function of the model parameters.

$$G(s) = \frac{Ke^{-\tau_d s}}{Ts + 1}, K_P = \frac{0.9T}{K\tau_d}, K_I = \frac{0.9T}{3.3K\tau_d^2} \quad (A18)$$

where T is the first order time constant, τ_d is the time delay, and K is the system gain.

Based on Eq. A17 and assuming a one breath time delay, we can then directly define the feedback gain parameters as a function of the timing parameters, where

$$K_P = \frac{0.9T_2}{T_B}, K_I = \frac{0.9T_2}{3.3T_B^2} \quad (A19)$$

and where T_B is one respiratory period. Parameterizing the feedback gains in terms of the reduced model amounts to designing the feedback controller to rapidly correct gas levels in the lung, while neglecting the body tissue levels. However, this controller is then inherently responsive enough to correct slower end-tidal deviations associated with body tissue dynamics and model errors.

The feedback parameters were then tested and varied in simulation to determine whether parameters based on the Ziegler-Nichols criteria were suitable when combining feedback and feedforward control. Based on simulations of step changes in desired arterial values, we found that both feedback parameters should be divided approximately by 2 to limit overshoots to <5%. For implementation in the end-tidal controller, this continuous feedback controller was converted to a discrete model with a one breath sampling period.

Ventilation compensation function. A ventilation compensation function additionally accounted for the direct input/output effect of changes in \dot{V}_A on end-tidal values. While the feedback control system does partially compensate for ventilation induced end-tidal errors, the controller is not designed to ideally reject these perturbations. In other words, the control system is designed based on the plant $P_{aCO_2}(s)/P_{iCO_2}(s)$ and not $P_{aCO_2}(s)/\dot{V}_A(s)$. During piloting, we found that feedback gains larger than those planned by Eq. A19 were necessary to compensate for the relatively rapid changes in end-tidal values due to changes in \dot{V}_A . However, these gains were too high in steady state conditions based on measured variability of end-tidal values. We therefore kept feedback gains small (based on Eq. A19) and adopted a ventilation compensation function to separately account for changes in measured \dot{V}_A ,

$$P_{iCO_2,corrected} = \left(P_{iCO_2,control} \cdot \dot{V}_A^* + P_{aCO_2,measured} \cdot (\dot{V}_A^* - \dot{V}_A) \right) / \dot{V}_A \quad (A20)$$

where \dot{V}_A^* is the baseline minute alveolar ventilation. Reflected in these equations is the concept that \dot{V}_A increases above baseline following end-tidal control are a response by the subject to return end-tidal values back to baseline by increasing the volume of inspiratory gas available for exchange in the lungs. The ventilation compensation function assigns a portion of the inspiratory volume to be at the measured arterial pressure, gas that theoretically does not contribute to gas exchange in the lung (22). The relative amount of gas at this arterial pressure relative to the controlled pressure, and thus the amount of CO_2 in the inspired air, increases proportionally with \dot{V}_A increases above baseline.

Measurement of Model Parameters

Quantification of timing parameters (Eq. A9) required estimation of subject specific and time dependent parameters. We estimated subject measures of lung and body tissue CO_2

volume based on age, height, and resting tidal volume. We also estimated time-dependent \dot{V}_A and \dot{Q} based on instantaneous V_T , f_R , and \dot{V}_E , measured with a five-breath running median filter.

Lung and body tissue CO_2 volume. The lung and body tissue CO_2 volumes were calculated based on relative values used previously, scaled by the relative ratio of each subject's lung volume to 2.5 liters (12, 16).

$$\begin{aligned} V_{ACO_2} &= V_{lung} \cdot (3.2/2.5) \\ V_{TCO_2} &= V_{lung} \cdot (15.0/2.5) \end{aligned} \quad (A21)$$

Subject lung volume is estimated as the functional residual capacity (FRC) plus half the resting tidal volume (20). FRC was estimated based on regression equations from (19):

$$\begin{aligned} \text{males : FRC(l)} &= \text{age(yr)} \times 0.01 + \text{height(m)} \times 2.34 - 1.09 \\ \text{females : FRC(l)} &= \text{age(yr)} \times 0.001 + \text{height(m)} \times 2.24 - 1.00 \end{aligned} \quad (A22)$$

Alveolar ventilation. Minute alveolar ventilation, \dot{V}_A , is equal to minute expired ventilation, \dot{V}_D , minus the dead space ventilation, V_T . Minute ventilation is calculated as the tidal volume, V_T , times the respiratory frequency, f_R .

$$\dot{V}_A = \dot{V}_E - \dot{V}_D \quad (A23)$$

$$\dot{V}_E = V_T \cdot f_R \quad (A24)$$

The total dead space volume includes the physiological dead space, which is the sum of the anatomical dead space and the alveolar dead space, and the mechanical dead space of the respiratory equipment (~253 ml). We estimated physiological dead space, which varies as a function of tidal volume, from the regression equations of Asmussen and Nielsen (1):

$$V_{D,phys} = 0.0656 \cdot V_T + 0.141 \text{ (liters, BTPS)} \quad (A25)$$

Dead space ventilation is then estimated as the total dead space times the respiratory frequency f_R .

$$\dot{V}_D = (0.0656 \cdot V_T + 0.141 + 0.253) \cdot f_R \quad (A26)$$

Cardiac output. We estimated cardiac output as a function of alveolar ventilation assuming that the ventilation perfusion-ratio \dot{V}_A/\dot{Q} was relatively constant around the resting and walking operating conditions tested. We used ratios of 0.87 and 1.68 for resting and light exercise, respectively, which were computed from published cardiopulmonary parameters (9).

ACKNOWLEDGMENTS

We are grateful to Jessica Selinger for manuscript comments and Michael Walsh for valuable technical and experimental advice.

GRANTS

This work was supported by a Michael Smith Foundation for Health Research Fellowship (to J. D. Wong) and the U.S. Army Research Office Grant W911NF-13-1-0268 (to J. M. Donelan).

DISCLOSURES

No conflicts of interest, financial or otherwise, are declared by the author(s).

AUTHOR CONTRIBUTIONS

S.M.O. and J.M.D. conception and design of research; S.M.O. performed experiments; S.M.O. analyzed data; S.M.O., J.D.W., and J.M.D. interpreted results of experiments; S.M.O. prepared figures; S.M.O., J.D.W., and J.M.D.

drafted manuscript; S.M.O., J.D.W., and J.M.D. edited and revised manuscript; S.M.O., J.D.W., and J.M.D. approved final version of manuscript.

REFERENCES

1. **Asmussen E, Nielsen M.** Physiological dead space and alveolar gas pressures at rest and during muscular exercise. *Acta Physiol Scand* 38: 1–21, 1956.
2. **Banzett RB, Garcia RT, Moosavi SH.** Simple contrivance “clamps” end-tidal PCO₂ and PO₂ despite rapid changes in ventilation. *J Appl Physiol* (1985) 88: 1597–1600, 2000.
3. **Battisti-Charbonney A, Fisher J, Duffin J.** The cerebrovascular response to carbon dioxide in humans. *J Physiol* 589: 3039–3048, 2011.
4. **Berne RM.** *Physiology*. St. Louis, MO: Mosby, 2004.
5. **Fierstra J, Sobczyk O, Battisti-Charbonney A, Mandell DM, Poublanc J, Crawley AP, Mikulis DJ, Duffin J, Fisher JA.** Measuring cerebrovascular reactivity: what stimulus to use? *J Physiol* 591: 5809–5821, 2013.
6. **Forster HV.** Exercise hyperpnea: where do we go from here? *Exerc Sport Sci Rev* 28: 133–137, 2000.
7. **Foster GE, Brugniaux JV, Pialoux V, Duggan CT, Hanly PJ, Ahmed SB, Poulin MJ.** Cardiovascular and cerebrovascular responses to acute hypoxia following exposure to intermittent hypoxia in healthy humans. *J Physiol* 587: 3287–3299, 2009.
8. **Hahn CE, Farmery AD.** Gas exchange modelling: no more gills, please. *Br J Anaesth* 91: 2–15, 2003.
9. **Hopkins SR, McKenzie DC, Schoene RB, Glenny RW, Robertson HT.** Pulmonary gas exchange during exercise in athletes. I. Ventilation-perfusion mismatch and diffusion limitation. *J Appl Physiol* (1985) 77: 912–917, 1994.
10. **Ito S, Mardimae A, Han J, Duffin J, Wells G, Fedorko L, Minkovich L, Katznelson R, Meineri M, Arenovich T, Kessler C, Fisher JA.** Non-invasive prospective targeting of arterial P(CO₂) in subjects at rest. *J Physiol* 586: 3675–3682, 2008.
11. **Jones NL, Robertson DG, Kane JW.** Difference between end-tidal and arterial PCO₂ in exercise. *J Appl Physiol Respir Environ Exercise Physiol* 47: 954–960, 1979.
12. **Khoo MC, Kronauer RE, Strohl KP, Slutsky AS.** Factors inducing periodic breathing in humans: a general model. *J Appl Physiol Respir Environ Exercise Physiol* 53: 644–659, 1982.
13. **Koehle MS, Giles LV, Curtis AN, Walsh ML, White MD.** Performance of a compact end-tidal forcing system. *Respir Physiol Neurobiol* 167: 155–161, 2009.
14. **Lind F, Hesser CM.** Breathing pattern and lung volumes during exercise. *Acta Physiol Scand* 120: 123–129, 1984.
15. **Liu Z, Vargas F, Stansbury D, Sasse SA, Light RW.** Comparison of the end-tidal arterial PCO₂ gradient during exercise in normal subjects and in patients with severe COPD. *Chest* 107: 1218–1224, 1995.
16. **Longobardo GS, Cherniack NS, Fishman AP.** Cheyne-Stokes breathing produced by a model of the human respiratory system. *J Appl Physiol* 21: 1839–1846, 1966.
17. **Ogata K.** *Modern Control Engineering*. Upper-Saddle River, NJ: Prentice-Hall, 1997.
18. **Peebles K, Celi L, McGrattan K, Murrell C, Thomas K, Ainslie PN.** Human cerebrovascular and ventilatory CO₂ reactivity to end-tidal, arterial and internal jugular vein PCO₂. *J Physiol* 584: 347–357, 2007.
19. **Quanjer PH, Tammeling GJ, Cotes JE, Pedersen OF, Peslin R, Yernault JC.** Lung volumes and forced ventilatory flows. Report Working Party Standardization of Lung Function Tests, European Community for Steel and Coal Official Statement of the European Respiratory Society. *Eur Respir J Suppl* 16: 5–40, 1993.
20. **Robbins PA, Swanson GD, Howson MG.** A prediction-correction scheme for forcing alveolar gases along certain time courses. *J Appl Physiol Respir Environ Exercise Physiol* 52: 1353–1357, 1982.
21. **Selinger JC, O'Connor SM, Wong JD, Donelan JM.** Humans can continuously optimize energetic cost during walking. *Curr Biol* 25: 2452–2456, 2015.
22. **Slessarev M, Han J, Mardimae A, Prisman E, Preiss D, Volgyesi G, Ansel C, Duffin J, Fisher JA.** Prospective targeting and control of end-tidal CO₂ and O₂ concentrations. *J Physiol* 581: 1207–1219, 2007.
23. **Snaterse M, Ton R, Kuo AD, Donelan JM.** Distinct fast and slow processes contribute to the selection of preferred step frequency during human walking. *J Appl Physiol* (1985) 110: 1682–1690, 2011.
24. **Swanson GD, Bellville JW.** Step changes in end-tidal CO₂: methods and implications. *J Appl Physiol* 39: 377–385, 1975.
25. **Wasserman K, Van Kessel AL, Burton GG.** Interaction of physiological mechanisms during exercise. *J Appl Physiol* 22: 71–85, 1967.
26. **Weil JV, Byrne-Quinn E, Sodal IE, Friesen WO, Underhill B, Filley GF, Grover RF.** Hypoxic ventilatory drive in normal man. *J Clin Invest* 49: 1061–1072, 1970.
27. **Wescott T.** *Applied Control Theory for Embedded Systems*. Burlington, VT: Newnes, 2006.
28. **West JB.** *Respiratory Physiology: The Essentials*. New York: Wolters Kluwer Health/Lippincott Williams & Wilkins, 2012.
29. **Zarrugh MY, Todd FN, Ralston HJ.** Optimization of energy expenditure during level walking. *Eur J Appl Physiol* 33: 293–306, 1974.
30. **Ziegler J, Nichols N.** Process lags in automatic control circuits. *Trans ASME* 65: 433–443, 1943.